Published in final edited form as:

J Urol. 2017 January ; 197(1): 255–261. doi:10.1016/j.juro.2016.06.100.

Evaluation of focal ablation of MRI-defined prostate cancer using MRI-controlled transurethral ultrasound therapy with prostatectomy as the reference standard

Elizabeth Ramsay[1], **Charles Mougenot**[2], **Robert Staruch**[3], **Aaron Boyes**[1], **Mohammad Kazem**[1], **Michael Bronskill**[1], **Harry Foster**[7], **Linda Sugar**[4], **Masoom Haider**[5], **Laurence Klotz**[6], and **Rajiv Chopra**[8,9]

[1]Physical Sciences Platform, Sunnybrook Research Institute, Toronto, Ontario, M4N 3M5, Canada

[2]Philips, Markham, Ontario, L6C 2S3, Canada

[3]Philips Research North America, 2 Canal Park, 3rd Floor, Cambridge, MA, 02141, USA

[4]Department of Anatomic Pathology, Sunnybrook Health Sciences Centre, Toronto, Ontario, M4N 3M5, Canada

[5]Department of Medical Imaging, University of Toronto, Sunnybrook Health Sciences Centre, Toronto, Ontario, M4N 3M5, Canada

[6]Department of Urology, Sunnybrook Health Sciences Centre, Toronto, Ontario, M4N 3M5, Canada

[7]Department of Anaesthesiology, Sunnybrook Health Sciences Centre, Toronto, Ontario, M4N 3M5, Canada

[8]Department of Radiology, University of Texas Southwestern Medical Center, Dallas, Texas, 75390-9061, USA

[9]Advanced Imaging Research Center, University of Texas Southwestern Medical Center, Dallas, Texas, 75390, USA

Keywords

Prostate Cancer; Transurethral Thermotherapy; MRI; High-Intensity Focused Ultrasound Ablation; HIFU

Corresponding Author: Rajiv Chopra, Department of Radiology, University of Texas Southwestern Medical Center, 5323 Harry Hines Blvd, Dallas, Texas, 75390-9061, USA, Rajiv.chopra@utsouthwestern.edu, p. 214-648-7745, f. 214-648-7767.

INTRODUCTION

In men with low-intermediate risk prostate cancer, minimally-invasive treatments may offer a treatment option for localized disease that is complementary to active surveillance[1]. This represents a middle ground between expectant management and radical treatment. Often delivered to a target or focal region of localized cancer, these treatments aim to destroy a subtotal volume of tissue within the gland, thereby decreasing damage to surrounding sensitive structures. In order for this treatment concept to be successful, two capabilities are required: 1) accurate localization of cancer within the prostate gland, and 2) treatment technologies which can achieve precise targeted tissue destruction within the gland. Multi-parametric MRI has been shown to provide accurate localization of tumors, and could be used to define targets for focal therapy[2–5]. Further, MR-ultrasound fusion biopsy systems offer more accurate mapping of cancer within the prostate[6–8].

In an attempt to leverage the strength of MRI for disease localization with the precision of tissue destruction offered by high intensity ultrasound energy, we have developed an MR-guided transurethral treatment for localized prostate cancer. The system is MR-compatible, and operates within the bore of a clinical scanner to generate a region of thermal ablation within the prostate gland. Real-time proton resonance frequency (PRF) shift MR thermometry[9] obtained during therapy is utilized to achieve accurate spatial control of tissue destruction. In previous phantom, animal, and pilot human trials, a spatial precision of 2–3 mm was demonstrated, with good potential for sparing surrounding tissues[10–15]. Important advantages of this approach compared with trans-rectal HIFU are treatment time reduction and the ability to treat larger glands[16].

A first-in-man treat and resect clinical study performed by Chopra et al[12] demonstrated the feasibility of coagulating prostate tissue using a prototype transurethral system, and of monitoring and controlling heating in the prostate during the procedure with MR thermometry. The treatments in this preliminary study, however, did not extend to the periphery of the prostate, and only a single plane of tissue was treated. More recently, a phase 1 study using a commercial transurethral system to coagulate the whole prostate gland was reported by Chin et al[17] demonstrating an acceptable safety profile and encouraging quality of life outcomes at 12 months. A three millimeter safety margin between the ablation boundary and prostate capsule was mandated in this study, which left up to 10% of the prostate volume untreated. Related human pilot studies have also shown MR-guided trans-rectal HIFU ablation to be feasible[18].

We describe the performance of a second-generation transurethral ultrasound therapy system in humans. This is the first clinical study performed in men prior to radical prostatectomy using a focal approach, combining MRI mapping of the tumor and subtotal prostate ablation. The necessary operating parameters required to achieve the desired therapeutic endpoint of complete tumor destruction and thermal coagulation up to the prostate capsule were determined, providing an important foundation for future studies with this technology.

MATERIALS AND METHODS

Human feasibility study

This clinical study was approved by the Research Ethics Board at Sunnybrook Health Sciences Centre and included men scheduled for radical prostatectomy who had an MR-visible, biopsy-proven stage T1 or T2a cancer with Gleason scores of ≤7 and PSA levels < 15ug/L. Six men provided informed consent, and five completed the study. The design was a treat and resect clinical investigation to determine the feasibility and safety of coagulating prostate tumors while extending treatment to the prostate boundary. The transurethral treatment was performed on the same day as the radical prostatectomy, with only 1 – 2 hours separating the two procedures. All prostatectomies were performed by the same surgeon (LK). Whole-mount hematoxylin-eosin (H&E)-stained histological sections obtained from the prostatectomy specimen were used to evaluate the extent of thermal coagulation and to compare this with MR imaging and thermometry measurements.

MR-controlled transurethral ultrasound therapy system

A prototype transurethral therapy system was integrated into a 3T MRI (Achieva, Philips Healthcare, Netherlands) for improved spatial resolution and temperature monitoring at the higher field strength[19]. The multi-element transurethral device consisted of eight contiguous planar transducer elements (5 mm long, 4 mm wide) which could operate independently at 4.5 MHz, 14.5 MHz, or a linear combination of the two frequencies. Once the transurethral applicator was inserted into the patient's urethra, its proximal end was attached to an MR-compatible positioning system which was affixed to the patient table of the MRI. This system contained an MR-compatible motor which rotated the applicator during treatment to direct energy to specific angular sectors within the gland. Subjects were treated in the supine position on the MR patient table, with imaging performed using a 32-channel cardiac RF coil array (Philips Healthcare, Netherlands). Degassed water was circulated independently through the transurethral applicator and an endorectal cooling device (ECD) using a custom-built flow circuit. Fig 1 shows photographs of the transurethral applicator (Fig 1a), ECD (Fig 1b) and an MR image (Fig 1c) indicating the positioning of these two devices in a patient.

The system was integrated with a modified version of an existing clinical MR-HIFU software platform (Sonalleve®, Philips Healthcare, Finland) to facilitate device registration, treatment planning and monitoring. The treatments were intended to achieve complete coagulation of tissue in an angular prostate segment which included the targeted tumor and extended to the capsule. During therapy, the software platform dictated acoustic powers, rotation rates, and frequencies based on a feedback control algorithm which analyzed the temperatures within the prostate gland and along the treatment boundary[20,21]. In return, the transurethral system transmitted information to the software platform in order to update the angular position of the device on the display as it rotated during treatment.

Treatment planning and delivery

Subjects were prepared for treatment on an MR table outside the magnet room. After administration of a spinal anaesthetic and insertion of the transurethral transducer and endorectal cooling devices, the patient bed was transported to and docked into the MR

scanner. Arterial oxygen saturation level, ECG and blood pressure were monitored throughout the treatment using an MR-compatible vital signs monitoring system (Expression Model 865214, Invivo, Gainesville, FL, USA). Core body temperature was monitored throughout the procedure using a fiber-optic thermometer (PicoM signal conditioner with OTG-M3000 sensor, OpSens, Quebec, Canada) inserted through a channel in the ECD to ensure contact with the inner rectal wall.

High-resolution 2D T2-weighted images and diffusion weighted (DWI) images were used for tumor identification and localization and treatment planning. The acquisition parameters for the MRI sequences used in the treatment protocol can be found in Supplemental Table 1. A target temperature was assigned (Fig. 2) to target boundaries defined by a uroradiologist (MH) using apparent diffusion coefficient (ADC) maps with a 5 mm angular extension on either side of the tumor. When the initially chosen target temperature of 54 °C proved insufficient to produce heating to the prostate boundary, it was increased to 56 °C and then 58 °C in later patients. Treatments used 2–6 transducers, depending on tumor extent (Table 1).

The treatment was delivered under temperature feedback control designed to maintain a constant temperature at the control boundary by adjusting the individual transducer powers and frequencies as well as the applicator rotation rate. Segmented EPI gradient echo thermometry images, co-planar with the planning images and aligned with the transducers (temporal resolution 6.3 s for 10 slices, spatial resolution 1.1mm), were obtained continuously over the course of treatment. Treatment times ranged from 9–35 minutes (Table 1).

Surgery and Correlation with Histology

Open radical prostatectomy using a standard nerve sparing technique was performed immediately following thermal treatment by an experienced prostatectomy surgeon (LK). The excised gland was painted to preserve orientation and paraffin-embedded for whole mount histological evaluation. Tissue sections of 5 μm were mounted on slides, stained with H&E and digitized. On each histology image, two thermal damage boundaries were traced for subsequent comparison with the MR temperature measurements: 1) the outer boundary of acute coagulative necrosis (ACN), inside which all cells underwent complete coagulative necrosis, and 2) the outer limit of thermal injury (OLTI), outside which there was no visual evidence of thermal damage. Post-treatment analysis included evaluation of the accuracy and precision of heating along the control boundary, the treatment accuracy with reference to histology, and an estimation of the maximum temperature at which cells were undamaged by treatment.

RESULTS

Axial temperature maps for all treated slices and all cases are shown in Figure 3. This overview indicates that treatments were successful in heating three dimensional target volumes having a wide variety of shapes, radii and number of slices. For each case except for P1, maximum temperatures of 60–80 °C were achieved throughout the planned treatment volume. In P1 the 4th active transducer failed, leading to a lack of treatment for that slice

(white arrow) and poor heating in the adjacent third slice. In P2 and P6 (green arrows), under-treatment was observed when the sector boundary was close to the edge of the prostate, where temperature measurements were unstable due to partial volume effects and the presence of large blood vessels. In P4, a region of under-treatment (yellow arrow) coincided with the location of a large calcification, while in the first slices of both P5 and P6, the presence of large benign prostatic hypertrophy (BPH) nodules led to uneven patterns of heating. Heating outside the planned treatment sector occurred in several cases. (P1 slice 2, P2 slice 4, P5 slice 2). This observation could be caused by heating of adjacent muscle, or be the result of unreliable thermometry outside the prostate boundary.

The mean temperature and spatial targeting accuracy are summarized in Table 2. For both metrics, perfect treatment would be indicated by an accuracy value of 0, with negative values indicating under-treatment and positive values indicating over-treatment. In all cases the average temperature at the control boundary was within error of the target temperature, with an overall average of −1.6 ± 4.8 °C. The average value of the mean spatial target accuracy was −1.5 ± 2.8 mm.

At radical prostatectomy performed 1–2 hours after the procedure, tissue consistency was within normal range, and there were no periprostatic adhesions, vascular engorgement or other tissue changes that could be related to prior ultrasound therapy.

Histology images for all six treatment planes of P6 are shown in Figure 4. An irregularly shaped tumor (yellow) located very close to the prostate boundary (blue) was present in five of the six slices. The white and black lines indicate the ACN and OLTI boundaries, respectively. Between these two boundaries, which are typically 1–2 mm apart, there was some heat-induced cell death and enough disruption of tissue structure that complete delayed cell death would have been expected if the prostate had not been removed[22]. The entire tumor fell within the OLTI boundary, with most of the cancer volume within the smaller ACN boundary. This was true of the index lesions in all five cases.

As the temperature of the control boundary (located 2 mm from the capsule) was increased, a progressive over-treatment was observed. Once the control temperature reached approximately 58 °C the over-treatment reached the prostate capsule, suggesting this was an appropriate target control temperature. The relationship between the amount of over-treatment and the control temperature is shown in Supplemental Figure 1.

DISCUSSION

This pilot study illustrates the feasibility of coagulating targeted angular sectors completely to the prostate capsule. Averaged over all sector angles, slices and subjects, the temperature control accuracy was −1.6 ± 4.8 °C, while the spatial targeting accuracy achieved was −1.5 ± 2.8 mm. This agrees with observations from recent clinical trials with similar technology[17]. The key requirements for this technology to achieve this performance include: 1) the ability to plan treatment sectors efficiently on a slice by slice basis, 2) independent control over power and frequency across the multi-element transducer[16,23], and 3) the

capability to perform 3D MR thermometry with sufficient temporal and spatial resolution to monitor the tissue temperature evolution during treatment[16,19,24,25].

Radical prostatectomy was performed immediately after treatment to assess treatment accuracy (the most clinically relevant metric) quantitatively by comparing cell damage observed in histological sections with temperature maps obtained from MR thermometry. The average treatment accuracy was found to be −0.4 ± 1.7 mm, within error of zero. The average temperature along the OLTI, i.e. the maximum temperature at which no significant thermal damage to cells occurs, was 54.0 ± 5.3 °C. All index tumors were within the outer limit of thermal injury. Finally, it was observed that when controlling the treatment based on MR thermometry measurements 2 mm inside the prostate capsule, a control temperature of 58°C was required to achieve full coagulation out to the boundary of the gland. This requirement for a higher temperature 2 mm inside the prostate gland arises primarily from unreliable PRF shift MR thermometry at the prostate capsule due to a mixed environment of water and fat based tissues.

Although this trial was similar in design to a previous feasibility conducted by our group, there were major differences in the technology used to generate the treatments. The treatments were performed in a 3T magnet, with full integration into the clinical MR-HIFU treatment planning software. Endorectal cooling was implemented to protect rectal tissues during treatment. A multi-element transducer operating at two frequencies was utilized, and multi-planar MR thermometry was used to deliver a volumetric treatment. This represents the likely clinical configuration of this technology for either whole gland or focal ablation.

There are several limitations to this study. The sample size was small, due to the difficulty in recruiting subjects eligible for the study and the substantial resource requirements involved in each case (ie, 3 hours in the MRI unit followed by 3 hours in the operating room). This small sample included prostates, however, with volumes ranging from 31 to 71 cc, containing interesting tissue features such as calcifications and BPH nodules. In the context of this first-in-man pilot study, the treatment parameters evolved during the study in an attempt to determine optimal strategies to coagulate tissue to the prostate boundary.

Anatomical features near and within the prostate can compromise treatment effectiveness. Pulsatile flow in large blood vessels adjacent to the prostate caused erroneous temperature readings, leading to poor temperature control at the target boundary. Blood flow in these extra-prostatic vessels may also have a local protective effect against thermal coagulation, as seen from the shape of the ACN boundary in slice 3 of patient 6 (fig. 4). Structural inhomogeneities within the prostate, such as calcifications and BPH nodules, can also lead to uneven heating patterns and failure to treat to the prostate boundary.

In conclusion, the results of this study demonstrate that MR-guided transurethral ultrasound therapy is capable of generating thermal coagulation within targeted 3D angular sectors within the prostate gland, and that coagulation can be produced to the prostate capsule in glands up to at least 70 cc. The ultrasound and thermal parameters necessary to achieve this goal were determined in this study and should prove useful for future clinical implementation of this technology.

Supplementary Material

Refer to Web version on PubMed Central for supplementary material.

Acknowledgments

The authors acknowledge financial support from the National Institutes of Health (1R21CA159550) for this clinical study. Rajiv Chopra also received research support from the Cancer Prevention and Research Initiative of Texas (R1308) during the preparation of this manuscript. The integration of the transurethral ultrasound therapy system with the HIFU treatment planning software was conducted through a collaborative research agreement between Sunnybrook Research Institute and Philips Medical Systems. Charles Mougenot and Robert Staruch are paid employees of Philips. Rajiv Chopra and Michael Bronskill are co-founders of Profound Medical, a company commercializing the transurethral ultrasound technology. Laurence Klotz serves on the clinical advisory board for Profound Medical. The company provided no support for these studies, and did not participate in the study design, execution or analysis of data. The authors would also like to thank Uri Lindner, Michael da Rosa, Ruby Endre, and Marlene Kebadjian for their assistance in subject recruitment and coordination on the day of treatments.

Key of Definitions for Abbreviations

ACN	acute coagulative necrosis
BPH	benign prostatic hypertrophy
ECD	endorectal cooling device
H&E	hematoxylin-eosin
HIFU	high intensity focused ultrasound
MR(I)	magnetic resonance (imaging)
OLTI	outer limit of thermal injury

References

1. Klotz L, Emberton M. Management of low risk prostate cancer-active surveillance and focal therapy. Nat Rev Oncol. 2014; 11:324–334.
2. Muller BG, van den Bos W, Brausi M, et al. Role of multiparametric magnetic resonance imaging (MRI) in focal therapy for prostate cancer: a Delphi consensus project. BJU Int. 2014; 114:698–707. Available at: http://www.ncbi.nlm.nih.gov/pubmed/24180365, accessed January 22, 2016. [PubMed: 24180365]
3. Rais-Bahrami S, Siddiqui MM, Turkbey B, et al. Utility of multiparametric magnetic resonance imaging suspicion levels for detecting prostate cancer. J Urol. 2013; 190:1721–7. Available at: http://www.ncbi.nlm.nih.gov/pubmed/23727310, accessed February 16, 2016. [PubMed: 23727310]
4. Oto A, Sethi I, Karczmar G, et al. MR imaging-guided focal laser ablation for prostate cancer: phase I trial. Radiology. 2013; 267:932–40. Available at: http://www.ncbi.nlm.nih.gov/pubmed/23440319, accessed March 29, 2016. [PubMed: 23440319]
5. Fütterer JJ, Briganti A, De Visschere P, et al. Can Clinically Significant Prostate Cancer Be Detected with Multiparametric Magnetic Resonance Imaging? A Systematic Review of the Literature. Eur Urol. 2015; 68:1045–53. Available at: http://www.ncbi.nlm.nih.gov/pubmed/25656808, accessed October 1, 2015. [PubMed: 25656808]
6. Costa DN, Pedrosa I, Donato F, et al. MR Imaging-Transrectal US Fusion for Targeted Prostate Biopsies: Implications for Diagnosis and Clinical Management. Radiographics. 35:696–708. Available at: http://www.ncbi.nlm.nih.gov/pubmed/25786055, accessed October 1, 2015.
7. Valerio M, Donaldson I, Emberton M, et al. Detection of Clinically Significant Prostate Cancer Using Magnetic Resonance Imaging-Ultrasound Fusion Targeted Biopsy: A Systematic Review. Eur

Urol. 2015; 68:8–19. Available at: http://www.ncbi.nlm.nih.gov/pubmed/25454618, accessed February 27, 2016. [PubMed: 25454618]

8. Siddiqui MM, Rais-Bahrami S, Turkbey B, et al. Comparison of MR/ultrasound fusion-guided biopsy with ultrasound-guided biopsy for the diagnosis of prostate cancer. Jama. 2015; 313:390–397. Available at: http://www.pubmedcentral.nih.gov/articlerender.fcgi?artid=4572575&tool=pmcentrez&rendertype=abstract, accessed September 23, 2015. [PubMed: 25626035]
9. Ishihara Y, Calderon A, Watanabe H, et al. A precise and fast temperature mapping using water proton chemical shift. Magn Reson Med. 1995; 34:814–823. [PubMed: 8598808]
10. Tang K, Choy V, Chopra R, et al. Conformal thermal therapy using planar ultrasound transducers and adaptive closed-loop MR temperature control: demonstration in gel phantoms and ex vivo tissues. Phys Med Biol. 2007; 52:2905–2919. [PubMed: 17473359]
11. Chopra R, Tang K, Burtnyk M, et al. Analysis of the spatial and temporal accuracy of heating in the prostate gland using transurethral ultrasound therapy and active MR temperature feedback. Phys Med Biol. 2009; 54:2615–2633. [PubMed: 19351975]
12. Chopra R, Colquhoun A, Burtnyk M, et al. MR Imaging-controlled Transurethral Ultrasound Therapy for Conformal Treatment of Prostate Tissue: Initial Feasibility in Humans. Radiology. 2012; 265:303–313. [PubMed: 22929332]
13. Partanen A, Yerram NK, Trivedi H, et al. Magnetic resonance imaging (MRI)-guided transurethral ultrasound therapy of the prostate: A preclinical study with radiological and pathological correlation using customised MRI-based moulds. BJU Int. 2013; 112:508–516. Available at: http://www.pubmedcentral.nih.gov/articlerender.fcgi?artid=3816743&tool=pmcentrez&rendertype=abstract, accessed September 20, 2015. [PubMed: 23746198]
14. Sammet S, Partanen A, Yousuf A, et al. Cavernosal nerve functionality evaluation after magnetic resonance imaging-guided transurethral ultrasound treatment of the prostate. World J Radiol. 2015; 7:521–30. Available at: http://www.pubmedcentral.nih.gov/articlerender.fcgi?artid=4697126&tool=pmcentrez&rendertype=abstract, accessed February 19, 2016. [PubMed: 26753067]
15. Diederich CJ, Stafford RJ, Nau WH, et al. Transurethral ultrasound applicators with directional heating patterns for prostate thermal therapy: in vivo evaluation using magnetic resonance thermometry. Med Phys. 2004; 31:405–413. [PubMed: 15000627]
16. Burtnyk M, Chopra R, Bronskill MJ. Quantitative analysis of 3-D conformal MRI-guided transurethral ultrasound therapy of the prostate: theoretical simulations. Int J Hyperthermia. 2009; 25:116–131. [PubMed: 19337912]
17. Chin, JL.; Billia, M.; Relle, J., et al. Magnetic Resonance Imaging-Guided Transurethral Ultrasound Ablation of Prostate Tissue in Patients with Localized Prostate Cancer: A Prospective Phase 1 Clinical Trial. Eur Urol. 2016. Available at: http://www.ncbi.nlm.nih.gov/pubmed/26777228, accessed January 18, 2016
18. Napoli A, Anzidei M, De Nunzio C, et al. Real-time magnetic resonance-guided high-intensity focused ultrasound focal therapy for localised prostate cancer: preliminary experience. Eur Urol. 2013; 63:395–398. Available at: http://www.ncbi.nlm.nih.gov/pubmed/23159454, accessed February 25, 2016. [PubMed: 23159454]
19. Ramsay E, Mougenot C, Köhler M, et al. MR thermometry in the human prostate gland at 3.0T for transurethral ultrasound therapy. J Magn Reson Imaging. 2013; 38:1564–1571. [PubMed: 23440850]
20. N'djin WA, Burtnyk M, Kobelevskiy I, et al. Coagulation of human prostate volumes with MRI-controlled transurethral ultrasound therapy: results in gel phantoms. Med Phys. 2012; 39:4524–36. Available at: http://www.pubmedcentral.nih.gov/articlerender.fcgi?artid=3412433&tool=pmcentrez&rendertype=abstract, accessed February 25, 2016. [PubMed: 22830784]
21. Chopra R, Burtnyk M, Haider MA, et al. Method for MRI-guided conformal thermal therapy of prostate with planar transurethral ultrasound heating applicators. Phys Med Biol. 2005; 50:4957–4975. [PubMed: 16237234]

22. Burtnyk M, Hill T, Cadieux-Pitre H, et al. Magnetic resonance image guided transurethral ultrasound prostate ablation: a preclinical safety and feasibility study with 28-day followup. J Urol. 2015; 193:1669–75. Available at: http://www.ncbi.nlm.nih.gov/pubmed/25464003, accessed September 20, 2015. [PubMed: 25464003]

23. Deardorff DL, Diederich CJ. Axial control of thermal coagulation using a multi-element interstitial ultrasound applicator with internal cooling. IEEE Trans Ultrason Ferroelectr Freq Control. 2000; 47:170–178. [PubMed: 18238528]

24. Pisani LJ, Ross AB, Diederich CJ, et al. Effects of spatial and temporal resolution for MR image-guided thermal ablation of prostate with transurethral ultrasound. J Magn Reson Imaging. 2005; 22:109–118. [PubMed: 15971190]

25. Chopra R, Wachsmuth J, Burtnyk M, et al. Analysis of factors important for transurethral ultrasound prostate heating using MR temperature feedback. Phys Med Biol. 2006; 51:827–844. [PubMed: 16467581]

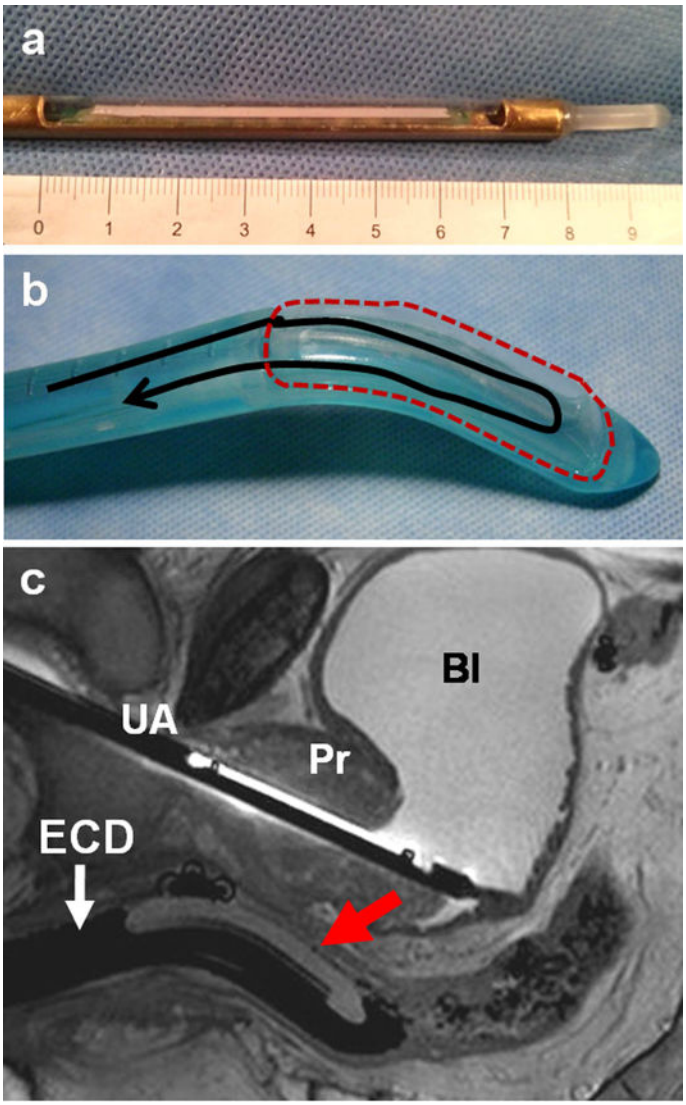

FIG. 1.

a) Photograph of the ultrasound applicator (UA). b) Photograph of the endorectal cooling device (ECD). The flow of cooling water is in the direction of the black arrow, while the red dotted line indicates a thin plastic window placed in the vicinity of the prostate gland. c) MR image showing the UA placed within the urethra in the prostate (Pr) with its tip in the bladder (Bl), and the ECD in the rectum with its plastic window (red arrow) oriented toward the prostate.

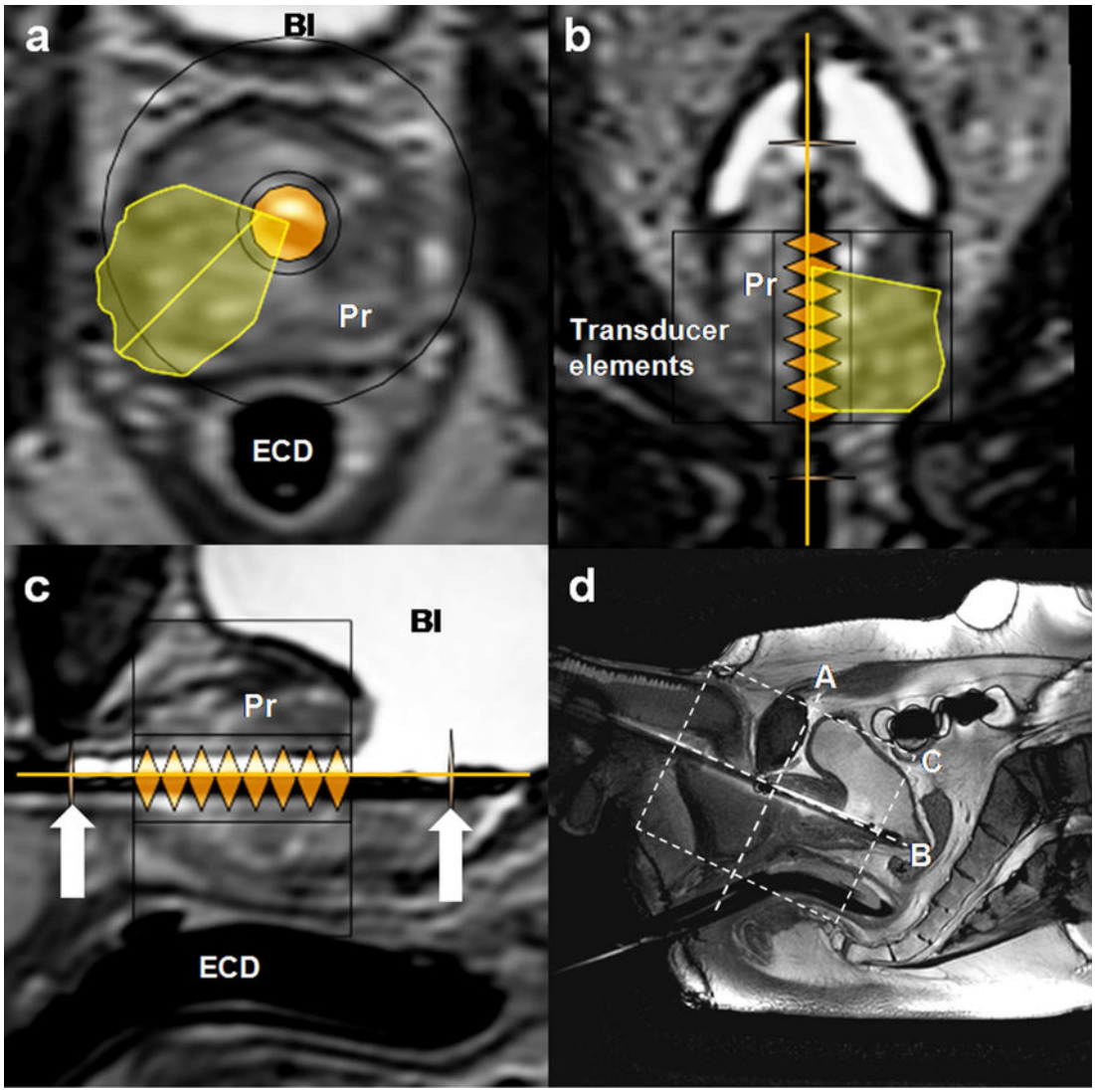

FIG. 2.

Panels a, b and c show axial, coronal and sagittal images reformatted from a T2w 3D TSE data set. The transducer elements are represented as orange diamonds. Two markers (indicated by thick white arrows) were aligned with applicator features as seen in the MR images to register the device with the planning software. A planned treatment sector is shown in yellow. Panel d shows a sagittal view with the transducer and ECD inserted. The dashed white box indicates the plane of image c, while the perpendicular lines indicate the planes of the images in panels a and b. Pr=prostate, Bl=Bladder, ECD=endorectal cooling device.

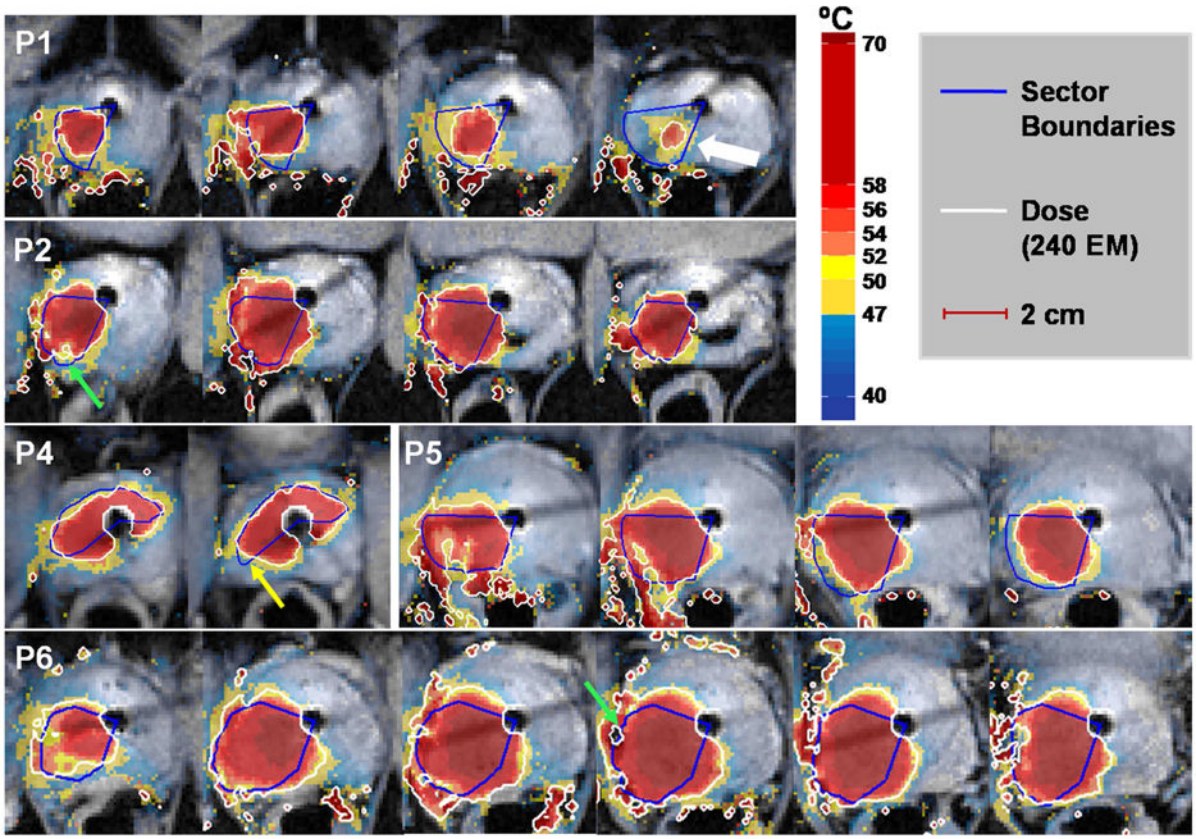

FIG. 3.

A collage of the axial maximum temperature maps at the end of treatment for all slices of all five completed cases in the study. Superimposed on each image are the 240EM dose line (white) and the boundaries of the treatment sector (blue). In the final slice of P1, the transducer element failed during treatment, resulting in insufficient heating in that location (white arrow).

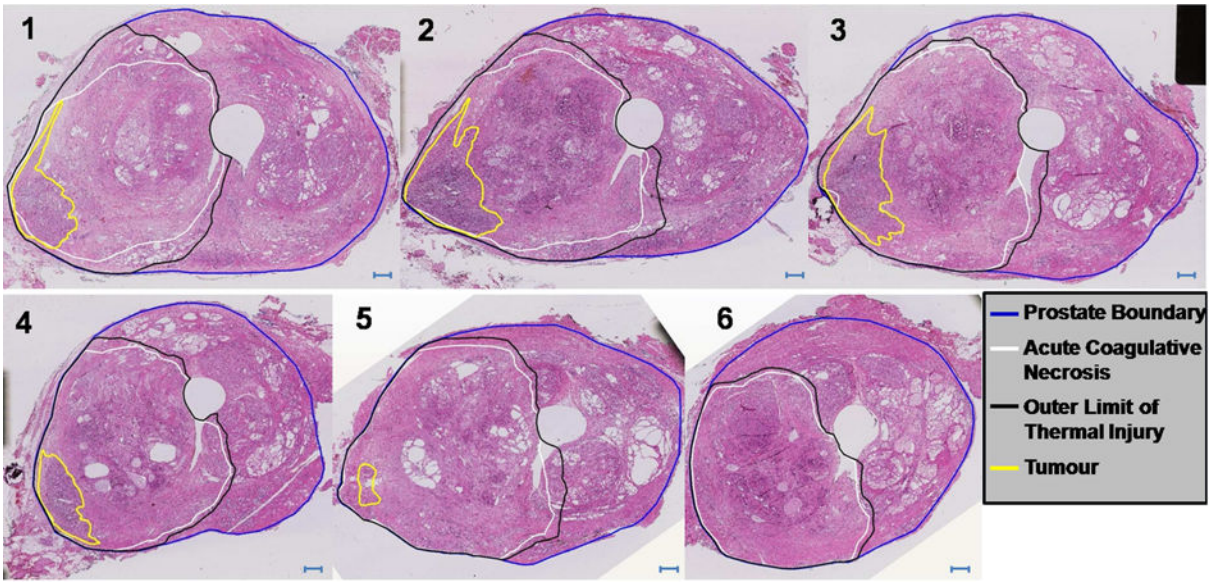

FIG. 4.

Histology images for all 6 slices of the treatment of Patient 6. Each image shows the prostate boundary (blue), the tumour boundary (yellow), the acute coagulative necrosis boundary (white) and the outer limit of thermal damage (black). Between the latter two boundaries, cells may not be immediately destroyed by the treatment, but are likely to undergo delayed necrosis. The scale bars indicate 2 mm.

Table 1

Patient and treatment sector information. Each column represents a different patient. Patient P3 was excluded because the transducer could not be inserted in the urethra.

Parameter/Patient	P1	P2	P4	P5	P6
Patient age (years)	69	53	57	74	64
Prostate volume (cc)	32	43	31	69	71
Number of treatment planes	4	4	2	4	6
Control temperature (°C)	54	54	56	58	58
Target volume (cc)	6.2	7.0	4.0	10.5	19.5
Treatment time (min)	12	9	24	13	35
Treatment rate (cc/min)	2.7	4.8	1.3	5.3	2.0
Mean radius (mm)	22.2	21.8	11.7	26.2	26.0
Radius range(mm)	16.3–26.1	14.4–24.8	8.0–22.0	15.6–31.0	11.8–35.1

Table 2

Summary of treatment results. Each column represents a different patient.

Metric/Patient	P1	P2	P4	P5	P6	Average
Mean temperature accuracy at control boundary (°C)	−2.9 ± 3.2	+0.7 ± 2.2	+1.3 ± 3.5	−5.2 ± 5.2	−3.1 ± 5.3	−1.6 ± 4.8
Mean spatial target accuracy (mm)	−1.9 ± 2.9	−0.6 ± 2.2	+0.3 ± 1.2	−3.8 ± 3.4	−2.30± 1.8	−1.5 ± 2.8
Mean treatment accuracy (mm)	−0.5 ± 1.9	−0.7 ± 1.7	0.5 ± 1.2	−1.7 ± 2.2	−0.1 ± 0.1	−0.4± 1.7
Mean temperature at outer boundary (°C)	51.7 ± 2.6	56.2 ± 3.1	49.7 ± 3.3	55.8 ± 7.4	56.6 ± 3.7	54.0 ± 5.3
*Dice Similarity Coefficient	0.81± 0.09	0.88± 0.03	0.81± 0.01	0.84± 0.05	0.94± 0.01	0.86± 0.04

*maximum, comparing temperature isotherms with ACN boundary